On the Southern Ocean CO2 uptake and the role of the biological carbon pump in the 21st century

Judith Hauck, Christoph Völker, Dieter A. Wolf-Gladrow, Charlotte Laufkötter, Meike Vogt, O. Aumont, Laurent Bopp, Erik T. Buitenhuis, Scott C. Doney, John P. Dunne, et al.

AGU PUBLICATIONS

Global Biogeochemical Cycles

RESEARCH ARTICLE
10.1002/2015GB005140

Key Points:
- Increase of CO_2 uptake driven by anthropogenic carbon, not by climate change
- A higher Revelle factor causes enhanced biologically driven CO_2 uptake in summer
- The southern Southern Ocean becomes more important for total CO_2 uptake

Supporting Information:
- Figures S1–S9 and Table S1
- Box Model S1 and Tables S2 and S3

Correspondence to:
J. Hauck,
judith.hauck@awi.de

Citation:
Hauck, J., et al. (2015), On the Southern Ocean CO_2 uptake and the role of the biological carbon pump in the 21st century, *Global Biogeochem. Cycles*, *29*, 1451–1470, doi:10.1002/2015GB005140.

Received 6 MAR 2015
Accepted 14 AUG 2015
Accepted article online 21 AUG 2015
Published online 23 SEP 2015

On the Southern Ocean CO_2 uptake and the role of the biological carbon pump in the 21st century

J. Hauck[1], C. Völker[1], D. A. Wolf-Gladrow[1], C. Laufkötter[2], M. Vogt[2], O. Aumont[3], L. Bopp[4], E. T. Buitenhuis[5], S. C. Doney[6], J. Dunne[7], N. Gruber[2], T. Hashioka[8], J. John[7], C. Le Quéré[5], I. D. Lima[6], H. Nakano[9], R. Séférian[10], and I. Totterdell[11]

[1]Alfred-Wegener-Institut, Helmholtz-Zentrum für Polar- und Meeresforschung, Bremerhaven, Germany, [2]Department of Environmental Sciences, ETH Zurich, Zurich, Switzerland, [3]Laboratoire de Physique des Océans, IRD, IUEM, 29280 Plouzané, France, [4]IPSL/LSCE, UMR8212, CNRS-CEA-UVSQ, Gif sur Yvette, France, [5]Tyndall Centre for Climate Change Research, University of East Anglia, Norwich, UK, [6]Woods Hole Oceanographic Institution, Department of Marine Chemistry & Geochemistry, Woods Hole, Massachusetts, USA, [7]Geophysical Fluid Dynamics Laboratory, Princeton, New Jersey, USA, [8]Japan Agency for Marine-Earth Science and Technology, Yokohama, Japan, [9]Meteorological Research Institute, Tsukuba, Japan, [10]CNRM-GAME, Toulouse, France, [11]Met Office, Exeter, UK

Abstract We use a suite of eight ocean biogeochemical/ecological general circulation models from the Marine Ecosystem Model Intercomparison Project and Coupled Model Intercomparison Project Phase 5 archives to explore the relative roles of changes in winds (positive trend of Southern Annular Mode, SAM) and in warming- and freshening-driven trends of upper ocean stratification in altering export production and CO_2 uptake in the Southern Ocean at the end of the 21st century. The investigated models simulate a broad range of responses to climate change, with no agreement on a dominance of either the SAM or the warming signal south of 44°S. In the southernmost zone, i.e., south of 58°S, they concur on an increase of biological export production, while between 44 and 58°S the models lack consensus on the sign of change in export. Yet in both regions, the models show an enhanced CO_2 uptake during spring and summer. This is due to a larger $CO_{2\,(aq)}$ drawdown by the same amount of summer export production at a higher Revelle factor at the end of the 21st century. This strongly increases the importance of the biological carbon pump in the entire Southern Ocean. In the temperate zone, between 30 and 44°S, all models show a predominance of the warming signal and a nutrient-driven reduction of export production. As a consequence, the share of the regions south of 44°S to the total uptake of the Southern Ocean south of 30°S is projected to increase at the end of the 21st century from 47 to 66% with a commensurable decrease to the north. Despite this major reorganization of the meridional distribution of the major regions of uptake, the total uptake increases largely in line with the rising atmospheric CO_2. Simulations with the MITgcm-REcoM2 model show that this is mostly driven by the strong increase of atmospheric CO_2, with the climate-driven changes of natural CO_2 exchange offsetting that trend only to a limited degree (~10%) and with negligible impact of climate effects on anthropogenic CO_2 uptake when integrated over a full annual cycle south of 30°S.

1. Introduction

The Southern Ocean acts as a window from the deep ocean to the atmosphere [*Russell et al.*, 2006; *Marshall and Speer*, 2012]. This is because the wind-driven strong upwelling brings carbon- and nutrient-rich deep water to the surface, where its gas content begins to equilibrate with the atmosphere. The high nutrient content fuels the growth of phytoplankton, but this growth is limited primarily owing to the widespread lack of the micronutrient iron [*De Baar et al.*, 1995; *Smetacek et al.*, 2012]. This makes the biological carbon pump in the Southern Ocean inefficient; i.e., there is more supply of inorganic carbon to the surface ocean by upwelling and mixing than there is inorganic carbon fixed into organic matter and exported to depth. This causes this region to be a strong source of natural CO_2 [*Mikaloff Fletcher et al.*, 2007; *Gruber et al.*, 2009], i.e., the carbon that existed in the atmosphere in preindustrial times. With the onset of industrialization, the strong increase in atmospheric CO_2 began to push growing amounts of anthropogenic CO_2 into the ocean [e.g., *Sarmiento et al.*, 1992; *Khatiwala et al.*, 2009, 2013]. This increase in the uptake of anthropogenic

CO_2 turned the Southern Ocean from a source of atmospheric CO_2 into a strong sink [*Hoppema*, 2004; *Gruber et al.*, 2009].

A telltale sign of the inefficient biological pump in the Southern Ocean is the presence of high concentrations of macronutrients that remain unused [e.g., *Sarmiento et al.*, 2004]. These excess macronutrients are exported northward and downward by the subduction of mode waters [*Sloyan and Rintoul*, 2001], enriching the nutrient content of the thermocline of the entire Southern Hemisphere [*Sarmiento et al.*, 2004]. As these laterally exported nutrients find their way back to the surface, they might fuel three quarters of the biological primary and export production in the low latitudes [*Sarmiento et al.*, 2004; *Marinov et al.*, 2006].

The Southern Ocean is also responsible for 40% of the global anthropogenic carbon uptake [*Mikaloff Fletcher et al.*, 2006; *Khatiwala et al.*, 2009] and is therefore an important player determining atmospheric CO_2 concentration and future climate. As is the case for the nutrients, most of this uptake is transported northward out of the Southern Ocean and to depth by the formation of mode and intermediate waters [*Mikaloff Fletcher et al.*, 2006], causing the most prominent accumulation of anthropogenic CO_2 to occur at around 30°S [*Sabine et al.*, 2004]. An additional conduit exists through the formation of bottom waters that takes place along the shelves of Antarctica, ventilating the abyss of the world's oceans and constituting a shortcut for transporting anthropogenic carbon into the deep sea [*van Heuven et al.*, 2014].

The recent southward shift and strengthening of the westerly winds associated with the progression toward a more positive phase of the Southern Annular Mode (SAM) [*Marshall*, 2003; *Thompson et al.*, 2011] increased the upwelling of carbon- and nutrient-rich deep waters but may also have increased the uptake of anthropogenic carbon. Thus, this may have perturbed the delicate balance between anthropogenic carbon uptake and outgassing of natural carbon in the Southern Ocean, possibly leading to less uptake per increase in atmospheric CO_2 [*Le Quéré et al.*, 2007; *Zickfeld et al.*, 2008; *Law et al.*, 2008; *Le Quéré et al.*, 2008; *Lovenduski et al.*, 2007; *Lenton and Matear*, 2007; *Verdy et al.*, 2007]. A relief of iron limitation, however, goes along with this enhanced upwelling. This constitutes a fertilization effect on the biological pump in summer that draws down a considerable amount of carbon and moderates the Southern Ocean's response to a higher carbon content through upwelling [*Hauck et al.*, 2013].

Climate model simulations suggested that the Southern Ocean might experience a further strengthening and a southward shift of the westerly winds in the 21st century [*Thompson et al.*, 2011; *Swart and Fyfe*, 2012; *Meijers*, 2014], i.e., that climate change will continue to push SAM toward its positive phase [*Zheng et al.*, 2013]. In the high-emission scenario RCP8.5, this strengthening is hardly mitigated by the recovery of the stratospheric ozone layer [*Meijers*, 2014]. The strengthening of the westerly winds leads to enhanced overturning and more mixing as the ocean would be less stratified. But at the same time, global warming and sea ice melt will make the surface of the Southern Ocean warmer and fresher [*Böning et al.*, 2008; *Meijers*, 2014], increasing upper ocean stratification and leading to a reduction of the maximum mixed layer depth (MLD) by up to 100 m [*Sallée et al.*, 2013]. This global warming signal is further intensified by changes in salinity reported for the Southern Ocean which is among the strongest salinity trends globally [*Durack and Wijffels*, 2010]. The freshening trend in the open ocean is possibly caused by a combination of changes in atmospheric fresh water fluxes, glacial melt water fluxes, and sea ice transport [*Purkey and Johnson*, 2013; *Rignot et al.*, 2008; *Haumann et al.*, 2014], and can impact deep convection events [*de Lavergne et al.*, 2014].

The physical changes expected in the future Southern Ocean will affect primary and export production [*Bopp et al.*, 2013; *Laufkötter et al.*, 2015; *Marinov et al.*, 2013] and carbon uptake, but different responses are plausible. The warming and freshening signal generally leads to a shoaling of the mixed layer (ML), keeping photo synthetically active phytoplankton in a higher light regime, presumably increasing biological carbon drawdown and CO_2 uptake from the atmosphere. The report of a ML shoaling driven by reduced heat loss in winter [*Sallée et al.*, 2013], however, is based on the analysis of the annual maximum MLD in the band of deepest winter ML along the northern edge of the Antarctic Circumpolar Current (ACC). Thus, it is unclear whether the increase in winds will invoke a deepening of the ML in some regions over the course of the year. A deepening of the ML would negatively affect the light availability for primary producers, but it would have a positive impact on the iron supply. The balance between the light and nutrient effects will determine the response of primary producers and the contribution of the biological carbon pump to CO_2 uptake.

Based on the physical changes reported above, we define four possible scenarios for biological responses: (1) The ML shoals due to global warming and this boosts export production thanks to a higher-light regime,

(2) the ML shoals due to global warming and this reduces primary production because less iron is available, (3) the ML deepens and overturning is enhanced due to stronger winds (SAM signal), and this enhances export production owing to additional iron input, (4) the ML deepens and overturning is enhanced due to stronger winds (SAM signal), and the thereby reduced light level leads to a decrease of primary and export production.

We analyze the RCP8.5 simulations from a suite of eight models from the Marine Ecosystem Model Intercomparison Project (MAREMIP) and Coupled Model Intercomparison Project Phase 5 (CMIP5) model intercomparison projects for their spatial and temporal trends in CO_2 uptake and export production and their drivers (sections 3.1 and 3.2). We thereby focus on the unraveling of how much biology contributes to changes of the Southern Ocean carbon sink (section 3.3). We are particularly interested in understanding (i) what drives the changes in export production, i.e., whether the SAM signal or the surface warming signal will be dominant; (ii) how important the biological carbon pump is for the Southern Ocean CO_2 sink in general and in the light of changes in export production; and (iii) what the expected changes are for the 21st century Southern Ocean carbon sink, taking into account the expected circulation changes and feedback processes.

We add to previous global studies of changes in primary and export production [*Bopp et al.*, 2013; *Laufkötter et al.*, 2015] by analyzing spatially and seasonally varying responses of the individual models in the Southern Ocean and by linking biological production to CO_2 uptake. We use an additional preindustrial simulation from one model and a simple box model to obtain a deeper understanding of the mechanisms at work where additional experiments to the MAREMIP/CMIP5 RCP8.5 simulation are needed and to provide an unambiguous link between 21st century climate change, biological response, and carbon fluxes.

2. Models and Data Analysis

CMIP5 and MAREMIP models. We compare model simulations for the period 2012 to 2100 which are forced by rising atmospheric CO_2 concentrations according to the RCP8.5 scenario [*Meinshausen et al.*, 2011]. We use a subset of models from the Marine Ecosystem Model Intercomparison Project (MAREMIP) [*Vogt et al.*, 2013; *Hashioka et al.*, 2013; *Sailley et al.*, 2013; *Laufkötter et al.*, 2015] and from the Coupled Model Intercomparison Project Phase 5 (CMIP5)[*Taylor et al.*, 2012]. We use all models that contain at least two phytoplankton functional types and provide all data necessary for our analysis (at least export production and CO_2 flux), resulting in eight model simulations. We use the first ensemble member for CMIP5 models (r1i1p1).

Selected models are either ocean-ice-ecosystem models (MITgcm-REcoM2, NEMO-PlankTOM5.3, MRI.COM-MEM) or fully coupled Earth system models (GFDL-ESM2M, IPSL-CM5A-LR, CNRM-CM5, CESM1, HadGEM2-ES, see Table 1). The ocean-ice-ecosystem models are forced with atmospheric fields from Earth system models after interaction with the ocean; thus, they implicitly include ocean-atmosphere feedbacks. Some models share the same ecosystem model (IPSL and CNRM: PISCES), others the same ocean model (IPSL, CNRM, PlankTOM5.3: NEMO but with different configurations and resolution, see, e.g., *Séférian et al.* [2013]), and some the same atmospheric forcing (REcoM2 and MEM: MIROC5, IPSL, and PlankTOM5.3: IPSL). In total, we analyze eight models with six different ocean general circulation models, seven ecosystem models, and six atmospheric models.

All ecosystem models have at least two phytoplankton and one zooplankton functional types and simulate the cycling of carbon and at least three nutrients (nitrate, silicate, and iron). All models except REcoM2 use the Redfield ratio for C:N uptake, and the implementation of stoichiometric ratios for C:Si:Fe:Chl varies widely between the models [see *Laufkötter et al.*, 2015]. The realization of nutrient uptake kinetics is equally diverse with MEM using optimum uptake kinetics [*Smith et al.*, 2009] and the other models either cell quota (GFDL) [*Geider et al.*, 1998] or a combination of cell quota and Michaelis-Menten kinetics (REcoM2, CESM1, PlankTOM5.3, HadGEM, IPSL, CNRM) [*Michaelis and Menten*, 1913].

The definition of MLD varies between the models where most models provide a monthly mean MLD estimate using a density criterion (Table 1). The threshold for the density criterion is either defined in units of kg m^{-3} (PlankTOM5.3, MEM, GFDL) or as a density threshold equivalent to a defined temperature change (CNRM, REcoM2) [*Kara et al.*, 2000]. MLD is defined as the depth where the buoyancy gradient to the surface is largest in CESM1 [*Large et al.*, 1997]. For IPSL, only the maximum monthly MLD defined by the mixing scheme is available. While the absolute numbers of MLD are hence not comparable, a deepening (shoaling) of the ML corresponds to less (more) light availability, independent of the MLD definition. Recalculating MLD off-line

Table 1. Overview of Models, Main References, and Criterion for Calculation of Mixed Layer Depth (MLD)[a]

Model Name	Ocean Model	Ecosystem Model	Reference	Atmospheric Forcing	MLD Criterion and Threshold
PlankTOM5.3	NEMO	PlankTOM5.3	*Buitenhuis et al.* [2013]	IPSL-CM5A-LR	Density[b], 0.03 kg m^{-3}
CESM1	POP	BEC	*Moore et al.* [2013]	Fully coupled	Max. buoyancy gradient[c]
MEM	MRI.COM	MEM	*Shigemitsu et al.* [2012]	MIROC5	Density, 0.125 kg m^{-3}
REcoM2	MITgcm	REcoM2	*Hauck et al.* [2013]	MIROC5	Density[d], $\Delta T = -0.8$ K
CNRM-CM5	NEMO	PISCES	*Aumont and Bopp* [2006]	Fully coupled	Density, $\Delta T = -0.2$ K
IPSL-CM5A-LR	NEMO	PISCES	*Aumont and Bopp* [2006]	Fully coupled	Mixing scheme
GFDL-ESM2M	MOM	TOPAZ	*Dunne et al.* [2013]	Fully coupled	Density[b], 0.03 kg m^{-3}
HadGEM2-ES	MetUM	diat-HadOCC	*Collins et al.* [2011]	Fully coupled	No data

[a]Note that IPSL MLD represents maximum MLD per month whereas the others are monthly average. CNRM and RecoM2 use a density-equivalent temperature criterion, i.e., $\Delta\sigma_\theta = \sigma_\theta(T + \Delta T, S) - \sigma_\theta(T, S)$ as in *Kara et al.* [2000].
[b]Refers to *de Boyer Montégut et al.* [2004].
[c]Refers to *Large et al.* [1997].
[d]Refers to *Kara et al.* [2000].

from monthly mean data is not accurate enough for studying seasonal MLD changes; hence, we use the online MLD calculation despite the differences in MLD definition.

The CO_2 exchange between atmosphere and ocean follows OCMIP protocols in all models [*Orr et al.*, 1999], and the dependence of wind speed is formulated according to *Wanninkhof* [1992] (IPSL, CNRM, CESM1, MEM, HadGEM) and includes chemical enhancement (REcoM2, PlankTOM5, GFDL). PlankTOM5.3 additionally applies a water vapor correction [*Sarmiento et al.*, 1992].

All models provide monthly mean data on export production, CO_2 flux into the ocean (F_{CO_2}) and sea ice area. Data on monthly mean surface nutrient limitation (calculated off-line from half-saturation values and nutrient concentrations in PlankTOM5.3, IPSL, CNRM, MEM) and MLD are available from all models except HadGEM. Throughout the manuscript we refer to the most limiting nutrient which was calculated from all possible nutrient limitations on every grid point before averaging spatially and temporally. Wherever data were not provided on a 1° × 1° grid, it was interpolated to this resolution using bilinear interpolation prior to analysis. Changes of properties are generally reported as the area-weighted mean state at the end of the simulation (2081 to 2100) minus the mean state at the beginning of the simulation (2012 to 2031).

Changes of all properties are reported when a two-sample *t* test rejected the null hypothesis that the data for the periods 2012–2031 and 2081–2100 come from independent random samples from normal distributions with equal means and equal but unknown variances at the 5% significance level. Changes of the multimodel mean are considered significant, when the range of the multimodel mean ±1 standard deviation does not include zero.

We perform two additional experiments with REcoM2, one (CONST) where we use the same atmospheric forcing fields as in the RCP8.5 simulation, but keep atmospheric CO_2 at the preindustrial level of 278 ppm throughout the model run (2012–2100). In a second simulation (ATMCO2) we use the same atmospheric CO_2 evolution as in RCP8.5 but use climatological atmospheric forcing. This allows us to differentiate between effects of climate change on F_{CO_2} and direct effects of the atmospheric CO_2 increase. Such experiments are only available for the RCP4.5 and 1% increase scenarios for some of the CMIP5 and not for MAREMIP models. We calculate climate change effects on F_{CO_2} as CLIM = RCP8.5 − ATMCO2, climate change effects on natural CO_2 flux as $CLIM_{nat}$ = CONST, climate change effects on anthropogenic CO_2 flux as $CLIM_{ant}$ = RCP8.5 − ATMCO2 − CONST, direct effects of atmospheric CO_2 increase as ATM = ATMCO2. Total changes in anthropogenic F_{CO_2} are then derived as $CLIM_{ant}$ + ATM.

Box model. We built a simple box model, consisting of three surface boxes where the southernmost boundary is the Antarctic continent and the northern boundaries of the boxes are at 58°S, 44°S, and 30°S, in line with previous studies of the Southern Ocean F_{CO_2} [*Mikaloff Fletcher et al.*, 2006; *Roy et al.*, 2011; *Lenton et al.*, 2013; *Hauck and Völker*, 2015]. The box south of 58°S contains the Antarctic Zone, the region 44–58°S includes large parts of the Subantarctic Zone and the Polar Frontal Zone with the Polar Front itself, and the region 30–44°S consists of the Subtropical Zone with a minor contribution of the Subantarctic Zone. The boxes are 100 m

deep to approximate the Southern Ocean surface layer which varies on spatial and temporal scales between approximately 30 and 100 m in summer and between 50 and 500 m in winter [*Sallée et al.*, 2010].

We calculate the wind-driven northward Ekman transport at the box boundaries with the MIROC atmospheric output fields which are also used as input for the MITgcm-REcoM2 model. In addition, we consider an 8 Sv (sverdrup; 10^6 m^3/s) flux of Antarctic Bottom Water (AABW) formation out of the surface for the southernmost box [*Orsi et al.*, 1999]. The upwelling or downwelling at the 100 m depth level is calculated as a mass balance from the surface Ekman transport and AABW formation.

The circulation in the box model considers only wind-driven circulation and a prescribed amount of bottom water formation. The upwelling calculated from the Ekman divergence is likely an upper bound as partial eddy compensation is not considered. The wind-driven Ekman transport across 44°S simulated by the box model is 28 Sv, in line with the 25–30 Sv range estimated by *Sloyan and Rintoul* [2001]. The physical transport is used together with the corresponding (deep or surface, dependent on the direction of transport) dissolved inorganic carbon (DIC) and alkalinity concentrations to calculate the tracer transports. We prescribe deep DIC and alkalinity concentrations, as well as temperature, salinity, gross primary production, respiration, remineralization (the latter three implicitly define export production) and sea ice fractional area as a monthly climatology obtained from MITgcm-REcoM2 output for the periods 2012 to 2031 and 2081 to 2100. Quadratic wind speed is taken directly from the MIROC5 atmospheric fields. We further prescribe atmospheric CO_2 with the mean values for 2012–2031 and 2081–2100 from the RCP8.5 scenario. The monthly surface DIC budget is calculated as the source minus sink (SMS) term

$$\mathrm{SMS(DIC)} = \mathrm{adv_h DIC} + \mathrm{adv_v DIC} - \mathrm{GPP} + \mathrm{resp} + \mathrm{remin} + F_{CO_2} \quad (1)$$

where we consider horizontal and vertical physical transports of DIC ($\mathrm{adv_h DIC}$ and $\mathrm{adv_v DIC}$), carbon drawdown (gross primary production, GPP), and release (respiration, resp, and remineralization, remin) by biology, all taken as output from REcoM2 and air-sea CO_2 flux F_{CO_2}. F_{CO_2} is calculated at every time step, following the same routine as in REcoM2 and is scaled by the amount of ice-free area in the box. The full equations and all parameters of the box model are given in the supporting information.

The box model captures the magnitude of annual F_{CO_2}, the timing of minimum and maximum F_{CO_2} and DIC concentrations reasonably well compared to REcoM2 (see Table S1 in the supporting information).

Box model experiments. The box model is basically a simplification of the MITgcm-REcoM2 model which allows us to easily perturb the system and to analyze the separate effects of processes that are inseparably tied together in REcoM2 and the other MAREMIP/CMIP5 models. For example, upwelling of carbon goes along with upwelling of nutrients in REcoM2, but here we can analyze the individual contributions of the increased speed of upwelling, increase of deep DIC concentration, and increase of export production as a result of more nutrient input.

The box model is run to equilibrium to simulate the average DIC budget in the period 2012 to 2031 ($\mathrm{CTRL_{start}}$) and 2081 to 2100 ($\mathrm{CTRL_{end}}$).

In our first experiment, we start from $\mathrm{CTRL_{start}}$ and perturb one of the following prescribed parameters individually: atmospheric CO_2, deep DIC concentration, temperature, export production, and wind speed. The perturbation of wind speed is applied separately to the equations of physical transport calculations and to the gas exchange formulation, so that we can further discern the effects of wind speed changes on the Ekman transport and on the gas exchange velocity. All parameters are perturbed to their mean state in the period 2081–2100 and are obtained from the REcoM2 RCP8.5 simulation, except wind speed, for which we apply a perturbation of +20% of the initial state as expected for the end of the century [*Downes and Hogg*, 2013]. We interpret the sum of the temperature, export production, and wind speed effects on F_{CO_2} as climate change effects which should be comparable to the CLIM results obtained from the REcoM2 simulations (see section 4.3).

In a second experiment, we switch off the effect of biology on the DIC budget completely, so that DIC is only affected by the physical transport and by gas exchange

$$\mathrm{SMS(DIC)} = \mathrm{adv_h DIC} + \mathrm{adv_v DIC} + F_{CO_2} \quad (2)$$

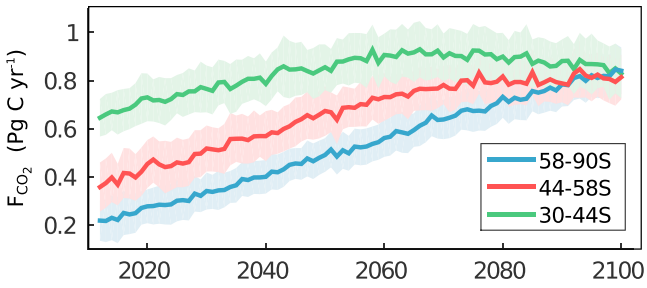

Figure 1. Time series of CO_2 flux (F_{CO_2}, positive = into the ocean, PgC yr^{-1}) in three subregions of the Southern Ocean as indicated in the figure. The lines show the multimodel mean, the shading depicts 1 standard deviation.

and hence F_{CO_2} is only affected by the physical transport of DIC. This experiment is conducted for both periods 2012–2031 ($NOBIO_{start}$) and 2081–2100 ($NOBIO_{end}$) and the contribution of biology to F_{CO_2} can be calculated as

$$BIO_{start} = CTRL_{start} - NOBIO_{start} \quad (3)$$

for the period 2012–2031 and equivalent for the period 2081–2100. One caveat of this approach is that by using deep DIC from a REcoM2 run with biology, there is a contribution of remineralization to deep DIC. We consider the changes in deep DIC from 2012–2031 to 2081–2100 to be mostly driven by changes in atmospheric CO_2 and only to a smaller extent by changes in remineralization. Hence, this experiment likely gives an upper bound on the role of the biological carbon pump and tests the transient response (before the adjustment in the vertical DIC gradient) to an extreme case, the complete cessation of biological export. This experiment is designed to elucidate how large the contribution of biology to the Southern Ocean carbon sink is today and how this is altered in the future. In contrast to experiment 1 that only accounts for the increase in export production, experiment 2 also includes interactions between biological carbon drawdown and decreasing buffer capacity [*Hauck and Völker*, 2015].

3. Results and Discussion

3.1. Multimodel Changes in Southern Ocean CO_2 Flux

The multimodel mean ocean CO_2 uptake (F_{CO_2}) shows distinctly different trends in the three major zones of the Southern Ocean south of 30°S (Figure 1). In the southernmost region, i.e., south of 58°S, the flux increases in a nearly linear manner between 2012 and 2100. In contrast, the region containing the Polar Front (44–58°S) shows a close to linear increase in F_{CO_2} only until 2075 and levels off thereafter. In the temperate region, i.e., between 30 and 44°S, F_{CO_2} reaches a maximum in the early 2060s and then decreases slightly toward the end of the century.

As a result, while the total F_{CO_2} south of 30°S doubles from 1.2 ± 0.3 PgC yr^{-1} to 2.5 ± 0.3 PgC yr^{-1}, the relative contribution of the three regions to the total uptake changes noticeably over the course of this century (Figure 1). In the beginning of the simulation, the region 30–44°S is responsible for three times the uptake in the region south of 58°S. At the end of the century, all regions contribute equally to total F_{CO_2} despite the difference in size among the regions (south of 58°S: 2.5 × 10^7 km^2, 44–58°S: 3.7 × 10^7 km^2, and 30–44°S: 4.5 × 10^7 km^2). The flux trends are significant in all individual models, regions, and seasons except for MEM in summer in the region 30–44° ($p < 0.05$).

In the considered high-emission scenario RCP8.5, atmospheric CO_2 increases steadily from 389 ppm in 2010 to 936 ppm in 2100 without any stabilization of emissions [*Meinshausen et al.*, 2011]. Therefore, the leveling-off and decrease of F_{CO_2} toward the end of the simulation in the regions north of 58°S have to be caused by physical, chemical, or biological feedbacks in the ocean.

Spring (September, October, November) and summer (DJF: December, January, February) contribute disproportionally more to the F_{CO_2} increase toward the end of the century than autumn (March, April, May) and winter (June, July, August) in the regions south of 44°S (Figure 2b). In the region 30–44°S the largest F_{CO_2} increase occurs during winter season. In summer, this region takes up less CO_2 at the end of the century (average 2081–2100) than at the beginning (2012–2031). This is true for all individual models except MEM

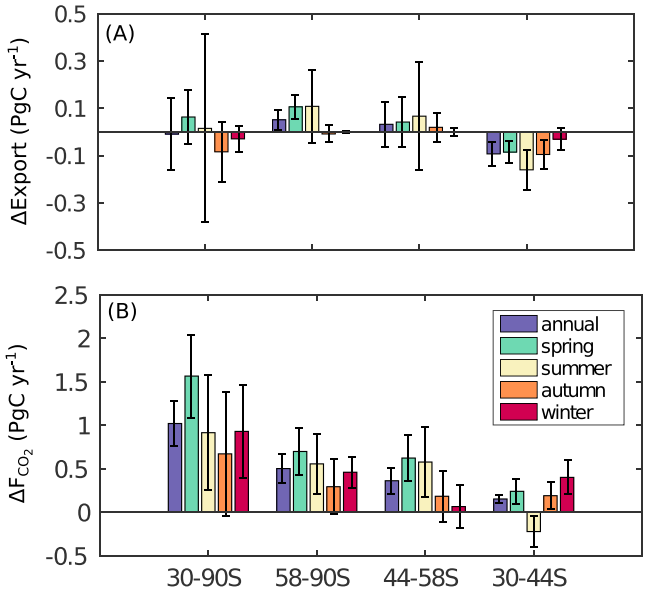

Figure 2. (a) ΔExport production and (b) ΔF_{CO_2}, both in units of PgC yr^{-1}, calculated as the average for period 2081–2100 minus the average for 2012–2031. Bars depict the multimodel mean, and error bars denote 1 standard deviation. If the error bar includes zero, the change is not significant.

(insignificant change), but the magnitude of the trend (range of $\Delta F_{CO_2} = -0.002$ to -0.04 PgC month^{-1}) and the point in time when F_{CO_2} starts to decline differs widely between the models (Figure 3).

What leads to the enhanced summer CO_2 uptake and to the strong meridional shift of the uptake pattern? In the following, we will explore changes in export production and whether they can explain the response in F_{CO_2} that we observe.

3.2. Multimodel Changes in Export Production and Its Causes

The largest increase in multimodel mean F_{CO_2} cooccurs with the multimodel mean increase in export production in spring and summer south of 44°S (Figure 2). In addition, the models agree on a reduction of export north of 44°S, exactly the same region where F_{CO_2} grew the least (despite the largest areal extent of the region), and where the ocean turned into a source of CO_2 in summer.

In the southernmost zonal band, i.e., south of 58°S, all models simulate an increase in export production in the Southern Ocean in line with *Bopp et al.* [2013] and *Laufkötter et al.* [2015], but timing varies among the models (Figures 4a and 4c). The largest increase is in summer (REcoM2 and MEM) or spring (all others), and all models except HadGEM project a significant increase in spring export. The multimodel mean export south of 58°S increases significantly by 0.05 ± 0.04 PgC yr^{-1} in the annual mean and by 0.1 ± 0.05 PgC yr^{-1} in spring. The relative annual change in export production varies between +2% in GFDL and +56% in MEM.

Between 44 and 58°S, two models (MEM and REcoM2) show a strong increase in export (0.5 and 0.4 PgC yr^{-1}, respectively) which peaks in summer, two models (CNRM and CESM1) show a weak to moderate increase (0.02 and 0.06 PgC yr^{-1}, respectively) that only occurs in spring, HadGEM shows an insignificant change in

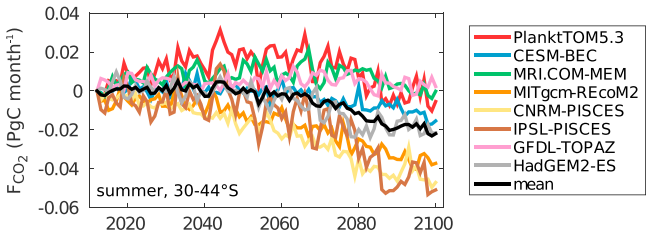

Figure 3. Time series of summer (DJF) F_{CO_2} between 30 and 44°S in eight models, normalized to the start value. Note that units are PgC month^{-1}. Negative numbers indicate outgassing. F_{CO_2} is significantly different in the period 2081–2100 from the period 2012–2031 in all models except MRI.COM-MEM.

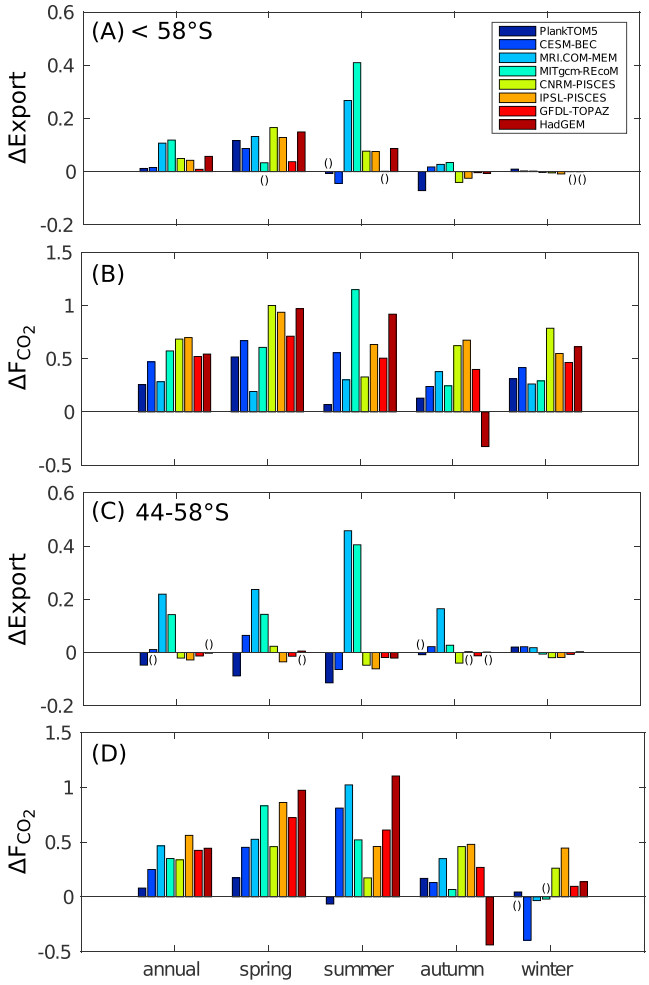

Figure 4. (a, c) ΔExport production and (b,d) ΔF_{CO_2}, both in PgC yr^{-1}, calculated as average in 2081–2100 minus average for period 2012–2031 for all individual models in the regions 44–58°S and south of 58°S (Figures 4c and 4d). All changes are significant except those marked with parentheses.

spring and weak decrease (−0.02 PgC yr^{-1}) in summer and three models (PlankTOM5, IPSL and GFDL) exhibit a significant decrease by −0.01 to −0.11 PgC yr^{-1} in export in spring and summer. The relative annual change in export production varies between −5% in PlankTOM5 and +32% in MEM. Due to the disagreement of models on the sign of export change, the multimodel mean export change is not significant in this region.

In the temperate region, i.e., between 30°S and 44°S, all models simulate a reduction of export (−0.03 to −0.18 PgC yr^{-1} in the annual mean and −0.03 to −0.26 PgC yr^{-1} in summer, Figure 5a), resulting in a multimodel mean decrease by −0.09 ± 0.05 PgC yr^{-1} in the annual mean and by −0.16 ± 0.09 PgC yr^{-1} in summer (Figure 2a). The relative annual change in export production varies between −19% in MEM and −3% in GFDL.

As we are interested in how the global warming signal (more stratification) and the SAM signal (less stratification, enhanced overturning) interact, and how the resulting MLD dynamics affect export production, we focus on light and nutrient availability as drivers for export changes. This is a valid approach, as export production is generally assumed to be equivalent to 'new production' [*Dugdale and Goering*, 1967], i.e., to the amount of nutrients that is entrained from below or provided by aeolian or fluvial input. In the high-nutrient-low-chlorophyll (HNLC) Southern Ocean, the limiting nutrient is iron [*De Baar et al.*, 1995; *Smetacek et al.*, 2012] and this feature is captured by all models but one (PlankTOM5), but changes in light availability through changes in MLD and changes in ice cover can modulate primary and export production. The strengthening of winds (SAM signal) leads to less stratification [*Carranza and Gille*, 2015] and enhanced Eulerian-mean meridional overturning circulation of the upper ocean, which is only partially balanced by eddies in CMIP5 models and high-resolution studies [*Downes and Hogg*, 2013; *Meredith et al.*, 2012]. While

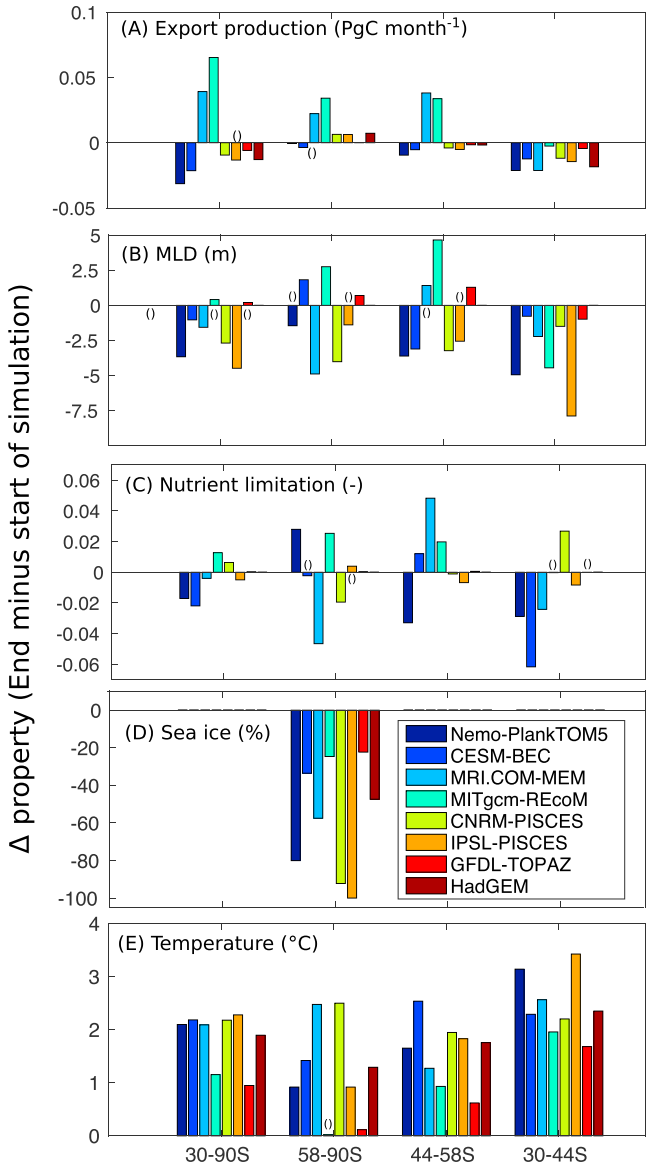

Figure 5. Summer (DJF) change between 2012–2031 and 2081–2100 for all models and regions: (a) export production, note that units are PgC month^{-1}, (b) MLD (m), (c) nutrient limitation factor for diatoms (dimensionless), negative numbers mean stronger nutrient limitation, positive numbers more nutrient availability, (d) sea ice area (%, December), (e) temperature (°C). All calculated as average 2081–2100 minus average 2012–2031. Changes are significant if not marked with parentheses. Note that IPSL MLD shows monthly maximum MLD, while the other models show monthly averages. Also note that nutrient limitation changes for GFDL are small in absolute values (<30°S: 0.2×10^{-3}, <58°S: 0.3×10^{-3}, 44–58°S: 0.6×10^{-3}, 30–44°S: -0.1×10^{-3}), due to the strong background nutrient limitation, relative changes are on the order of 5%. All changes are significant except those marked with parentheses.

there is model agreement that overturning will strengthen until 2100 [*Downes and Hogg*, 2013], seasonal changes of MLD have not been studied so far, despite their strong effect on chlorophyll concentrations in the Southern Ocean [*Carranza and Gille*, 2015].

A deeper ML leads to less light and more nutrient availability. Most models show a band of deeper winter ML somewhere between 40°S and 60°S and shallower MLD north and south of that (not shown) enhancing the winter nutrient input. Here we focus on summer MLD changes as an indicator of light changes and nutrient supply within the growing season (Figure 6). In all models except CNRM, summer MLD increases in parts of the Southern Ocean until the end of the century. This change is mostly confined to south of 50°S (Figure 6), but not in all models does this lead to a mean deepening when averaged over the regions south of 58°S or

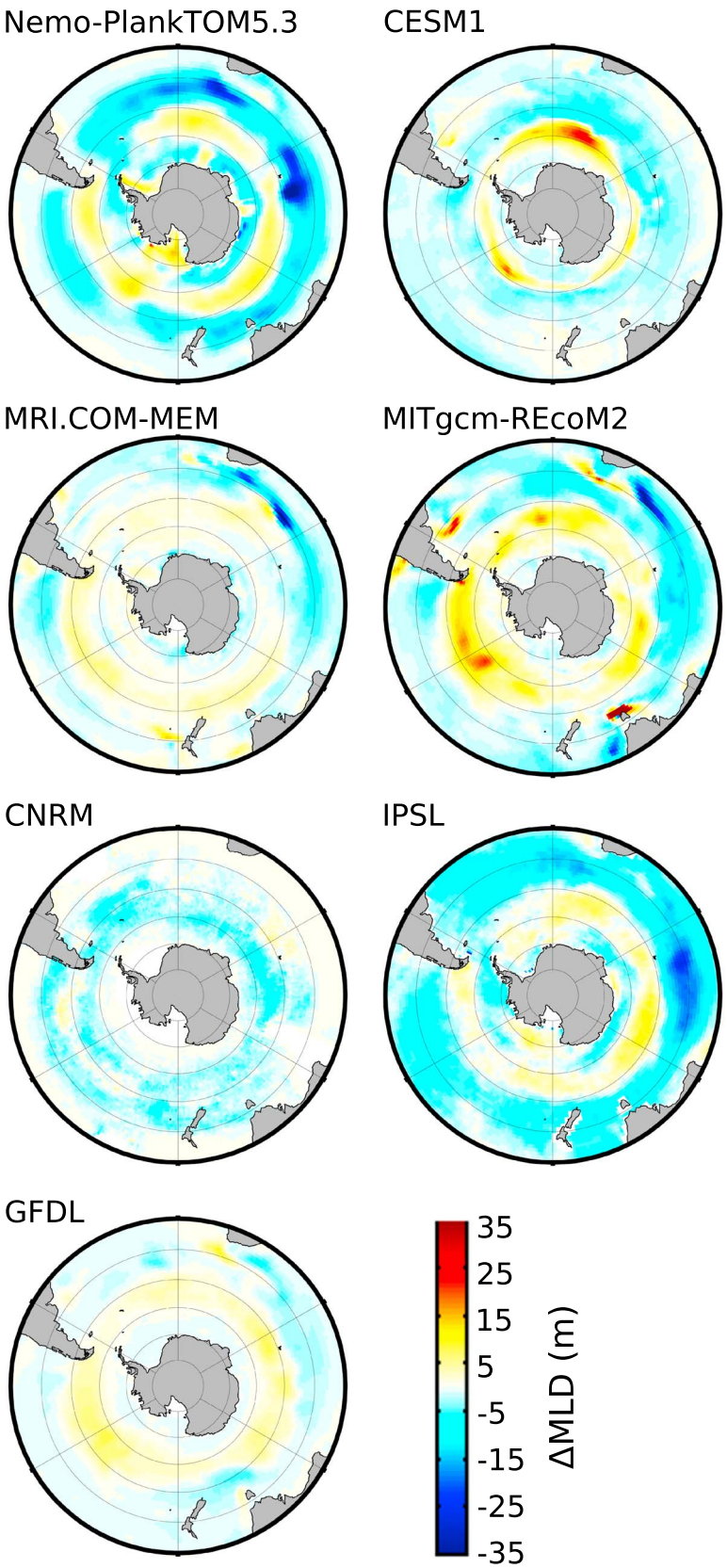

Figure 6. Changes in minimum (summer) mixed layer depth (MLD) between 2012–2031 and 2081–2100 for seven models as indicated in the figure. Positive values indicate deepening of the mixed layer. See Table 1 for MLD definitions.

Table 2. Summary of Summer (DJF) Changes in MLD (ΔMLD), Diatom Nutrient Limitation (Δnut) and Export Production (ΔEP)[a]

Model	ΔMLD	Δnut	ΔEP	SAM or gw	Nut-/or Light-Driven
South of 58°S					
PlankTOM5.3	(–)	+	(–)	?	?
CESM1	+	(–)	–	?	?
MEM	–	–	+	gw	light
REcoM2	+	+	+	SAM	nut
CNRM	–	–	+	gw	light
IPSL	(–)	(+)	+	?	?
GFDL	+	+	(+)	SAM	(nut)
44–58°S					
PlankTOM5.3	–	–	–	gw	nut
CESM1	–	+	–	?	?
MEM	(+)	+	+	(SAM)	nut
REcoM2	+	+	+	SAM	nut
CNRM	–	–	–	gw	nut
IPSL	(–)	–	–	(gw)	(nut)
GFDL	+	+	–	SAM	light
30–44°S					
PlankTOM5.3	–	–	–	gw	nut
CESM1	–	–	–	gw	nut
MEM	–	–	–	gw	nut
REcoM2	–	(–)	–	(gw)	(nut)
CNRM	–	+	–	?	?
IPSL	–	–	–	gw	nut
GFDL	–	(–)	–	(gw)	(nut)

[a]For MLD, plus (+) means that MLD becomes deeper ; for Δnut, plus (+) means the limitation factor increases; for EP, plus (+) indicates an increase in export production. Parentheses indicate that the change is not significantly different from zero ($p < 0.05$). The combination of plus (+) for ΔMLD and plus (+) for Δnut indicates that the SAM signal is dominant, marked as SAM in the respective column. The combination of minus/minus (–/–) indicates that the global warming signal (gw) is dominant. If the SAM signal is dominant and export increases (decreases), the change is nutrient driven (light driven), global warming signal dominant, and export increase (decrease) corresponds to light-driven (nutrient-driven) response. Inconclusive combinations are marked with a question mark (?). Note that the sign of the nutrient limitation response and its significance is the same whether diatoms or nanophytoplankton are considered, except for GFDL 30–44°S where the response is only significant for nanophytoplankton.

44–58°S (Figure 5b). The CNRM model is already too stratified at the end of the historical hindcast [*Séférian et al.*, 2013].

In summer, three out of seven models show a deepening of the ML in the region south of 58°S (CESM1, REcoM2, GFDL), two show an average shoaling (MRI.COM-MEM, CNRM), and two models show no significant change (IPSL, NEMO-PlankTOM5.3). Between 44°S, and 58°S, again, two models (MITgcm-REcoM2, GFDL) simulate a deeper MLD at the end of the century, three models (NEMO-PlankTOM5, CESM1, CNRM) exhibit a shallower MLD, and the changes in IPSL and MRI.COM-MEM are not significant (Figure 5b and Table 2). North of 44°S, the models agree on a reduction of summer MLD by 1 to 8 m (Figure 5b).

The models that simulate a summer deepening of the ML in the southernmost region (CESM1, REcoM2, GFDL) show the lowest reduction in summer sea ice area (20–30%, Figure 5d). This indicates that the simulated freshening by a general sea ice reduction as warming proceeds or by altered sea-ice production, transport and melting [*Haumann et al.*, 2014] can determine the balance between the SAM (wind forcing) and global warming (thermal and salinity forcing) effects on stratification in the models.

As expected, shoaling of the ML is generally coupled to a stronger nutrient limitation, while an ML deepening alleviates the nutrient limitation (Figure 5c and Table 2). Only in two cases (CESM1 44-58°S, CNRM 30-44°; Table 2) a significant shoaling of the ML is accompanied by higher nutrient availability. This indicates that changes in MLD are often but not always a proxy for changes in nutrient limitation. Changes in horizontal advection, for example, can lead to enhanced nutrient input without being detectable as MLD changes.

Note that Figure 5c presents absolute changes in nutrient limitation, and the changes in GFDL, even if significant, are so small that they are indistinguishable from zero by eye on the given scale. The present-day nutrient limitation, however, is stronger in GFDL than in the other models, so that the relative changes are of the order of 5% as in the other models.

The latitudinal bands of all models can be grouped according to the main mechanism that drives export changes. We do that exemplarily for summer where the effect of export on F_{CO_2} is relevant (Table 2 and Figure 5), and note that other mechanisms can be dominant in other seasons. Nutrient-driven models exhibit an increase in export production along with a relief in nutrient limitation (REcoM2 south of 58°S, MEM, REcoM2 in the region 44–58°S) or a decrease in export production as nutrient limitation is enhanced (PlankTOM5, CNRM, IPSL 44–58°S). In other models, light-driven changes dominate and the increase in light due to a shoaling of the ML outweighs reduced nutrient input and export production increases (MEM, CNRM south of 58°S) or the decrease in light as the ML deepens can reduce export (GFDL 44–58°S). The increase in export production south of 58°S is further positively affected by the retreat of sea ice in all models by 20 to 100% (Figure 5d), providing a larger area for production as the models do not account for biological production within and underneath the sea ice.

South of 58°S, two models predict the SAM (REcoM2, GFDL) and another two models the global warming effect (MEM and CNRM) on export production to be dominant (Table 2). Similarly, two models project that the SAM (GFDL, REcoM2) and two others that the global warming signal (PlankTOM5.3, CNRM) will be dominant, respectively, in the region 44–58°S. In the other models, the changes are either not significant or inconclusive (see caption of Table 2).

In the region 30–44°S, the models agree on a reduction of summer export (all eight models) driven by stronger nutrient limitation (four of seven models; two models show insignificant change and one projects weakening of nutrient limitation), despite a higher light availability as the ML shoals (all seven models). The GFDL model shows an insignificant change in diatom nutrient limitation term but a significant increase in nanophytoplankton nutrient availability (not shown), supporting this conclusion.

While our approach can explain changes of export production in most models, it works less well in the following cases. We can only hypothesize (i) why the CNRM model projects an increase in nutrient and light availability, but an export decrease in the region 30–44°S, (ii) why the increase of nutrients at an insignificant change of MLD south of 58°S in PlankTOM5.3 does not result in an increase in export, (iii) why the deepening of the ML in CESM1 south of 58°S does not trigger an increase in nutrient availability, and (iv) why the higher light and nutrient availability in CESM1 in the region 44–58°S does not lead to higher export production (Figure 5 and Table 2). This might be caused by changes in temperature, grazing [*Laufkötter et al.*, 2015], and/or ecosystem composition (i, ii, and iv) or by nonlinearities in the system that we loose when averaging over the specified regions (i–iv). The decoupling of stratification and nutrient availability in CESM1 south of 58°S (iii) can be explained by intensified advective iron fluxes [*Misumi et al.*, 2014], and the nonresponsiveness of PlankTOM5 to increased nutrient availability (ii) could be due to unaltered and strong light limitation conflicting with *Venables and Moore* [2010] who showed that light limitation does not constrain biological production in summer.

3.3. Can Changes in Export Production Explain the Changes in CO_2 Flux?

We expect that monthly time series of start (2012–2031) export production and F_{CO_2} south of 44°S are highly and positively correlated, reflecting the seasonal cycle as the largest scale of variability in the Southern Ocean which is a sink for CO_2 in summer [*Lenton et al.*, 2013] driven by biological carbon uptake [*Bakker et al.*, 1997; *Takahashi et al.*, 2002]. We observe, however, that the models differ widely in how strong regionally averaged monthly time series of export and F_{CO_2} are correlated (Figure 7). Only three models show a significant and positive correlation between F_{CO_2} and export (REcoM2, CESM1, HadGEM) in the regions 44–58°S and south of 58°S. All models except CNRM show a significant positive correlation in at least one region. The models that share NEMO as the ocean model (IPSL, CNRM, PlankTOM5) show a tendency to negative correlations.

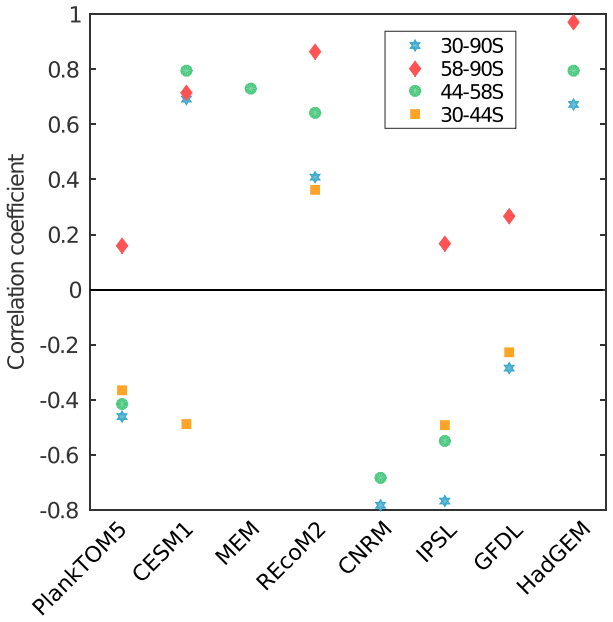

Figure 7. Correlation between monthly time-series at start of simulation (2012–2031) of export production and F_{CO_2}. Shown are correlation coefficients for significant correlations ($p < 0.05$).

Other factors, such as upwelling or temperature, seem to affect the seasonal cycle of F_{CO_2} more than biology in these models, deviating from the general picture that biological carbon drawdown is the main driver for seasonal variations in F_{CO_2} in the Southern Ocean [e.g., *Takahashi et al.*, 2002]. The poor representation of the seasonal cycle of F_{CO_2} in the Southern Ocean in some models was shown earlier [*Lenton et al.*, 2013]. While this questions the adequate representation of the processes driving F_{CO_2} in the models with negative correlation between export and F_{CO_2}, it is also a first indication that export production might not be able to fully explain the changes in F_{CO_2} in all models.

While models agree on increasing export and summer F_{CO_2} in the southernmost region (Figures 4a and 4b), it is evident that in the region 44–58°S other processes must be at work, as also models that show a decrease in export in spring/summer can have a pronounced seasonal peak in F_{CO_2} (GFDL, HadGEM, IPSL, CESM1, Figures 4c and 4d).

If the changes in F_{CO_2} were caused by enhanced biological production due to climate change, this signal should be apparent in the simulation of the natural CO_2 (C_{nat}) flux conducted with REcoM2 (CONST). Indeed, more uptake of C_{nat} occurs in summer (south of 58°S) and in summer and autumn (44–58°S, Figure S1 and 8b). As upwelling of carbon-rich deep water would work in the opposite direction (less uptake of C_{nat}), we reckon that climate change leads to more (micro)nutrient input that sustains a higher biological production in

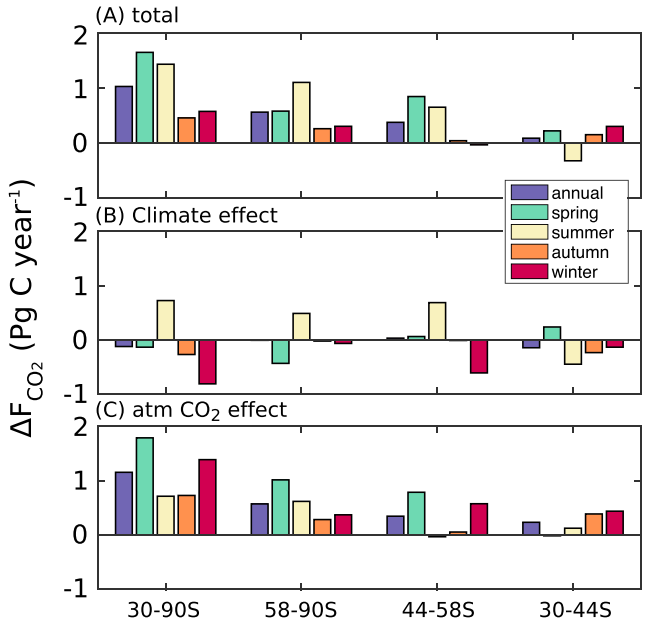

Figure 8. Mean change of (a) total F_{CO_2}, (b) F_{CO_2} due to climate effects on natural and anthropogenic carbon, and (c) F_{CO_2} due to increase of atmospheric CO_2 between the periods 2012–2031 and 2081–2100 in REcoM2 in different seasons. See Figure S1 for contributions of natural and anthropogenic F_{CO_2}.

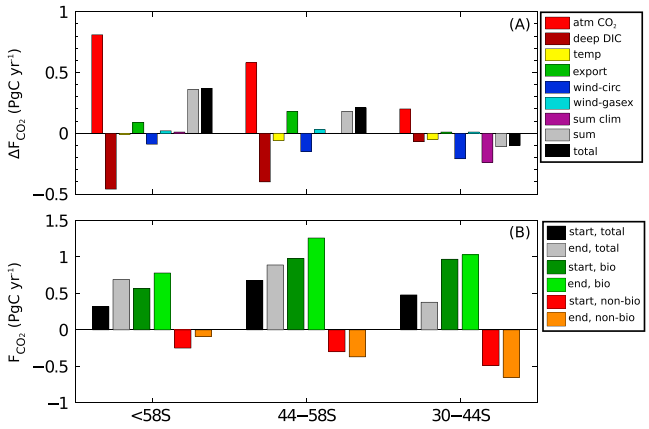

Figure 9. Box model results. (a) Experiment 1: ΔF_{CO_2} due to perturbation of one parameter at a time from the state 2012–2031 to the state 2081–2100. sum clim: sum of temperature, biology, wind speed effects on circulation, and gas exchange; sum: sum of all individual perturbations; total: when all are perturbed simultaneously. Difference between sum and total due to nonlinearities, i.e., interaction between two perturbations. (b) Experiment 2. Total (black, grey), biologically driven (dark and light green), and nonbiologically driven (red, orange) F_{CO_2} for the periods 2012–2031 ("start") and 2081–2100 ("end"). Nonbiologically driven F_{CO_2} is from box model run with biology switched off. Biologically driven F_{CO_2} is the difference between box model simulation with and without biology. Negative numbers indicate flux out of the ocean.

summer which overcompensates the DIC input, thus leading to a more efficient carbon pump. As a result, more C_{nat} is taken up from the atmosphere [*Hauck et al.*, 2013]. In winter, however, more upwelling leads to enhanced outgassing of C_{nat} and these two processes cancel out in the region 44–58°S (ΔC_{nat} = −0.006 PgCy^{-1}). In the other regions, there is a small residual (ΔC_{nat} = south of 58°S: −0.06 PgC y^{-1}, 30–44°S: −0.05 PgC y^{-1}), indicating that circulation changes will lead to a weak outgassing signal of C_{nat} of 0.11 PgC y^{-1} in the total Southern Ocean south of 30°S (about 10% of total F_{CO_2} changes). Climate effects on anthropogenic carbon fluxes also show opposing trends among seasons, with increasing $F_{C_{ant}}$ in summer to winter south of 58°S, in spring and summer in the region 44–58°S, and in spring in the temperate region (30–44°S). In the annual mean for the total SO (south of 30°S) climate effects on $F_{C_{ant}}$ average out to less than 1% of total F_{CO_2} changes (Figure S1). The largest part of total F_{CO_2} change occurs directly due to atmospheric CO_2 increase (Figure 8c), and climate-driven F_{CO_2} changes are small in comparison (Figure 8b+c) and account for 11% of the total F_{CO_2} changes.

In order to understand the relative importance of physical and biological processes on F_{CO_2} in the RCP8.5 simulation, we use the simple box model as introduced in section 2.

The results of experiment 1, where we perturb the individual parameters to their mean state in the period 2081–2100 as obtained from REcoM2, are illustrated in Figure 9a. Each bar shows how much F_{CO_2} is altered by perturbing one process in the respective region. An increase in F_{CO_2} is caused by the increase of export production and of atmospheric CO_2. While increased export production directly reduces the DIC concentration, the increase of atmospheric CO_2 affects F_{CO_2} by the combination of at least two counteracting effects: (i) higher atmospheric CO_2 increases the CO_2 gradient between ocean and atmosphere, leading to more CO_2 uptake and (ii) the Revelle factor increases as more CO_2 is taken up and limits further uptake (see discussion in section 4.2). In addition, the faster gas exchange at higher wind speed has a minor positive effect on F_{CO_2}. F_{CO_2} is negatively affected by warming, increased Ekman transport, and higher DIC concentration below the surface layer. The warming effect is straightforward as the ocean can hold less CO_2 at higher temperatures. Increased Ekman transport and pumping bring up more carbon-rich deep water and thereby increase the surface DIC concentration. This is even more important as the deep DIC concentration will increase as a result of atmospheric CO_2 rise. In reality, the increase of atmospheric CO_2 is inseparably tied to deep DIC concentration, yet the box model allows us to look at these contributions separately.

The most important drivers for changes in F_{CO_2} are therefore increasing carbon concentrations in the atmosphere and the subsurface ocean. Changes in F_{CO_2} due to export production are of similar magnitude as F_{CO_2} changes due to wind-driven circulation changes (label "wind-Ekman" in Figure 9a) except north of 44°S where F_{CO_2} changes due to changes in physical carbon transport dominate because export changes are small.

Temperature effects on carbonate chemistry and wind speed effects on gas exchange are of minor importance. The area over which gas exchange occurs is increased by the recession of sea ice extent. This does not alter F_{CO_2} significantly in the box model (therefore, this bar is not shown in Figure 9a), yet this might underestimate the real effect of sea ice as the boxes are assumed to be well mixed and high DIC concentrations cannot accumulate under the ice as is the case in the real world and in the general circulation models.

There is only a small residual between the sum of all individual perturbations (labeled "sum" in Figure 9a) and the response when all parameters are perturbed simultaneously (labeled "total" in Figure 9a), indicating that the individual responses can be added up linearly. The climate change effects (sum of temperature, wind, export changes, and "sum clim" label in Figure 9a) are comparable to the changes in CLIM in REcoM2 in the sense that they are small in the regions south of 58°S and 44–58°S and larger and negative in the region 30–44°S although this effect is stronger in the box model (Figure 8c; see discussion in section 4.3).

The temperature change in REcoM2 that is taken as forcing for the box model is among the weaker responses of the MAREMIP/CMIP5 models (Figure 5e). As an additional test, we perturb the initial surface temperature field in the box model by +2°C which is reached by some models (Figure 5e) to estimate the impact of temperature change on F_{CO_2}. This would increase the effect of temperature change on F_{CO_2} from −0.01 to −0.05 PgC yr^{-1} in the southernmost region (south of 58°S). It would reduce the T effect on F_{CO_2} somewhat in the region 44–58°S (from −0.06 to −0.03 PgC yr^{-1}) and in the temperate region (from −0.05 to −0.01 PgC yr^{-1}, 30–44°S). In combination with the simulation of relatively large export changes in REcoM2, the relative effects of changes in export production and temperature on F_{CO_2} will vary among models.

The role of biology for the Southern Ocean F_{CO_2} is further emphasized by box model experiment 2 where the box model is run with and without biology for the periods 2012–2031 and 2081–2100. The difference in F_{CO_2} between the runs with and without biology is then ascribed to the biological carbon pump (labeled "bio" in Figure 9b). In contrast to experiment 1, the change of the biological contribution to F_{CO_2} between 2012–2031 and 2081–2100 is not only due to the increase in export production but also due to interaction with other changing processes.

Figure 9b demonstrates that the modern and future Southern Ocean would turn into a source of CO_2 to the atmosphere if biology did not sequester CO_2 (labeled "nonbio" in Figure 9b). The biologically driven F_{CO_2} increases (more uptake) from the period 2012–2031 to the period 2081–2100 by 0.2, 0.28, and 0.07 PgC yr^{-1} (difference between "start, bio" and "end, bio" in Figure 9b) in the regions south of 58°S, 44–58°S and 30–44°S, respectively. This increase is more than twice as large as the effect due to increasing export production (from experiment 1, Figure 9a), and we attribute this difference (0.12, 0.1, and 0.05 PgC yr^{-1} from south to north) to the larger $CO_{2\,(aq)}$ drawdown in the less buffered system at the end of the century [*Hauck and Völker*, 2015] (see also section 4.2).

4. Synthesis

In the following, we will summarize and discuss all results of the different models (MAREMIP/CMIP5 RCP8.5 simulation, REcoM2 experiments RCP8.5, CONST and ATMCO2, and box model) jointly to address the specific questions that we posed in section 1: What are the drivers for changes in export production? What is the impact of the biological carbon pump on CO_2 uptake? How will the Southern Ocean carbon sink change and what are the most important processes?

4.1. Drivers for Changes in Export Production

All models show an increase of export somewhere in the Southern Ocean, in line with previous studies [*Laufkötter et al.*, 2015; *Bopp et al.*, 2013], but patterns and timing differ widely. North of 44°S, the warming signal dominates the models' MLD response, i.e., the ML shoals (Figure 5b and Table 2). It remains unclear whether the SAM signal, as characterized by deeper mixed layers and more nutrients, or the global warming signal with shallower mixed layer, less sea ice, and more light will be dominant in the future south of 44°S (Figure 5b and Table 2). The models also differ in whether they simulate the system changes to be mainly nutrient or light driven (Table 2).

The differences between the models are affected by differences in all their components: atmospheric forcing, ocean circulation model, and ocean ecosystem model. The models' simulations of a deeper or shallower mixed layer are driven by the physical model and the atmospheric forcing (wind, thermal, and freshwater forcing). Whether two models that both simulate a deeper mixed layer give the same export response depends

on the physical settings (e.g., eddy diffusion and entrainment of nutrients) but also on the ecosystem model (e.g., initial nutrient gradient between surface and deep ocean, remineralization, and ligands). Different projections of future export production can therefore not be traced back to certain settings in the model setup due to the large number of differences. The models with the largest export changes (MEM and REcoM2) share the same atmospheric forcing, but the sign of MLD change is opposite south of 58°S. There is no agreement on the sign of change of nutrient limitation terms between CNRM and IPSL that share the same ocean and ecosystem model and differ only slightly in the configuration of the ocean model but use different ice and atmospheric models. The largest agreement in terms of nutrient limitation changes is between PlankTOM5.3 and IPSL (same sign of change in all regions) that use the same ocean model and atmospheric forcing (once coupled online, once as external forcing after interaction with the ocean), but the changes are considerably stronger in PlankTOM5.3. Interestingly, IPSL and PlankTOM5.3 also simulate very similar MLD responses, reflecting the importance of the MLD dynamics and the role of the ocean model and atmospheric forcing. We cannot distinguish fully coupled from uncoupled models by means of a statistical *t* test in terms of the magnitude of their change in export production at the 5% significance level.

In summary, export changes can largely be explained by bottom-up control in these models, yet further evaluation and improvement of modeled mixed layer depth dynamics is required to obtain a more definite conclusion on the future dominance of the SAM or the global warming signal including the freshening trend. Future work should address the questions why and how the summer mixed layer that determines the light and nutrient availability for phytoplankton production changes in all regions, how the differences between the models can be explained, and what their main drivers are (wind, thermal, or freshwater forcing). MEM and REcoM2 use the same atmospheric forcing, yet the average summer MLD change south of 58°S is positive in REcoM2 (deepening) and negative in MEM (shoaling) indicating that the state of the ocean plays a role in addition to the atmospheric forcing and highlighting also the importance of evaluation and improvement of present-day MLD representations in ocean models [*Sallée et al.*, 2013].

4.2. Impact of the Biological Pump on CO_2 Uptake

The multimodel mean comparison of export production and F_{CO_2} in the RCP8.5 simulation suggests that the relatively stronger increase of F_{CO_2} in summer is linked to the increase of export production (Figure 2). The analysis of the REcoM2 RCP8.5 and CONST simulations indeed shows that there is a stronger summer CO_2 uptake in the future even when considering only climate effects (Figures 8 and S1). We explain this with the SAM's fertilizing effect as the enhanced mixing and overturning due to stronger winds bring up additional nutrients and stimulate biological production [*Hauck et al.*, 2013]. This mechanism can nearly balance the circulation-driven outgassing of natural carbon [*Le Quéré et al.*, 2007; *Lenton and Matear*, 2007; *Lovenduski et al.*, 2007; *Verdy et al.*, 2007] that would be even larger otherwise.

Yet the spring and summer increase in export production cannot explain the stronger seasonality of F_{CO_2} in all models. The enhanced spring/summer CO_2 sink is also apparent in models that simulate a decrease in spring and summer export production in the region 44–58°S (Figures 4c and 4d). This is caused by the switch to a less well-buffered system (i.e., a higher Revelle factor $R = \frac{\Delta pCO_2}{pCO_2} / \frac{\Delta DIC}{DIC}$) that leads to a larger drawdown of $CO_{2\,(aq)}$ and hence F_{CO_2} into the ocean per amount of biological production at the end of the century in all three regions of the Southern Ocean. This effect on $CO_{2\,(aq)}$ is larger in magnitude than the effect of increased export production until 2100 [*Hauck and Völker*, 2015] and most probably leads to the seasonally distinct increase in F_{CO_2} in the individual models and in the multimodel mean (Figure 2). The box model based on REcoM2 confirms that the biologically driven CO_2 uptake will grow approximately twice as fast as the increase in export production in all three regions (Figure 9) and suggests that this interaction between biology and buffer factor might contribute 0.27 PgC yr^{-1} to the total ΔF_{CO_2} in the Southern Ocean box model with all its limitations (see next section).

In summary, all models show an enhanced spring or summer CO_2 uptake south of 44°S pointing to the increased importance of the biological carbon pump in a less well-buffered system in the southern Southern Ocean that also constrains the potential of CO_2 uptake further north.

4.3. Changes of the Southern Ocean CO_2 Uptake in the 21st Century

The contribution of the three defined areas (south of 58°S, 44–58°S, and 30–44°S) to the total F_{CO_2} will change in the second half of the 21st century, with the more southerly areas' relative contributions increasing. This might well reflect the balance between the two effects of a higher Revelle factor, namely, the general reduction of F_{CO_2} and the increase of the biologically driven seasonal F_{CO_2}. The two regions south of 44°S have

a stronger seasonal CO_2 drawdown by biological production, and therefore, the biologically driven Revelle effect [*Hauck and Völker*, 2015] plays a larger role here than farther north. The additional uptake in the south limits additional uptake farther north, given that northward surface transport prevails. We propose that this mechanism and the timing of the bloom being spring rather than summer north of 44°S in REcoM2 [*Hauck and Völker*, 2015] can explain the outgassing of anthropogenic CO_2 by the end of the century in REcoM2 (Figure S1) and the multimodel mean decrease of summer F_{CO_2} in this region (Figure 2).

REcoM2 and the box model agree that climate-driven changes in F_{CO_2} are small (10% in REcoM2) relative to the increase in F_{CO_2} driven by rising atmospheric CO_2 south of 44°S. Winter outgassing of carbon-rich deep water is partly balanced by enhanced biological production, leaving a residual outgassing of natural CO_2 of 0.11 PgC yr^{-1} (2081–2100 compared to 2012–2031) south of 30°S, whereas an additional 1.15 PgC yr^{-1} C_{ant} will be taken up in REcoM2. The total ΔF_{CO_2} of 1.03 PgC yr^{-1} in REcoM2 is in the center of the ranges of ΔF from the MAREMIP/CMIP5 models (0.53 to 1.41 PgC yr^{-1}) with a projected multimodel mean change of 1.02 ± 0.26 PgC yr^{-1}.

It has been argued that the increase in wind speed can also lead to enhanced F_{CO_2} once the surface DIC concentration is higher than the deep DIC concentration [*Zickfeld et al.*, 2008; *Le Quéré et al.*, 2008]. Indeed, the surface DIC concentration exceeds the deep DIC concentration at the end of the century in the region 44–58°S in the box model and the wind speed effect on Ekman transport in this state enhances F_{CO_2} (not shown). However, this effect is not seen in REcoM2, where the average surface concentration of DIC is lower than the deep DIC concentration throughout the year in all regions. The MAREMIP/CMIP5 models agree (all models except CNRM that differs already at the beginning of the simulation) that the deep DIC concentration will remain higher than the surface DIC concentration in all three regions throughout the 21st century (Figures S2–S8). The discrepancy between MAREMIP/CMIP5 models and the box model is likely to be related to changes in the deep circulation that are not simulated with the box model. This is in agreement with *Ito et al.* [2015] who showed that warming and freshening of Antarctic surface water will cause a weakening of the deep overturning circulation that in turn increases biological carbon storage in the Southern Ocean. All models but one agree that the largest DIC change will occur at the surface, which is also in agreement with the large increase of preformed carbon storage [*Ito et al.*, 2015] due to atmospheric CO_2 increase, except PlankTOM5.3 where DIC increases strongest between 500 m and 2000 m. The steepness of the DIC gradient at the end of the simulation, however, varies widely between the models. To identify the mechanisms at work in all individual models is beyond the scope of this work and should be the subject of future research [see also *Ito et al.*, 2015]. It will further be important how the alkalinity gradient between surface and deep ocean evolves and whether the ratio of carbon to alkalinity in upwelled/entrained water will change.

The limitation of the box model to capture the vertical DIC gradient is also revealed in the role that climate change effects have in the region 30–44°S. The box model suggests that climate change effects reduce the total F_{CO_2} by 0.24 PgC yr^{-1}, whereas it is only reduced by 0.15 PgC yr^{-1} in REcoM2 in this region. We conclude that the system is sensitive to the concentration gradient between surface and deep DIC, and this will be important for determining the sign of the wind effect on F_{CO_2}. The box model, however, represents a crude simplification of the circulation. A possible explanation for this difference in results is that the assumption of well-mixed boxes leads to a too fast DIC transport via northward Ekman transport overestimating the circulation effect on F_{CO_2} in the north. This leads to strong F_{CO_2} in the south resulting in high DIC concentrations and less F_{CO_2} farther north. Other factors are the accumulation of DIC below the sea ice that occurs in REcoM2, but not in the box model and deep circulation changes that are not included in the box model [*Ito et al.*, 2015].

5. Concluding Remarks

With the suite of eight marine ecosystem models and a box model we identified the most important drivers for the future CO_2 uptake (F_{CO_2}) in the Southern Ocean (plus increase in F_{CO_2}, minus decrease in F_{CO_2}). The largest impact is by the increase of atmospheric pCO_2 (+) by its direct (+) and indirect effect of subsurface DIC increase (−). All models show a larger effect of biological production on CO_2 uptake by interaction with high Revelle factor (+) [*Hauck and Völker*, 2015]. Increase of export production (+), the effect of surface warming on F_{CO_2} (−), and enhanced upwelling of carbon-rich deep water at stronger winds (−) are of similar magnitude, and relative importance varies between models, whereas the effect of wind speed on gas exchange (+) is small.

Mixed-layer depth dynamics can explain the changes in export in most regions and models, but other factors such as temperature and grazing might control the response in the remaining models. We find all possible scenarios (shoaling and deepening of mixed layer with dominance of either nutrient or light control) in at least one model and region. There is no agreement among models whether the system south of 44°S will be predominantly controlled by the global warming signal or by the SAM signal. In the region 30–44°S the global warming signal with a shallower mixed layer prevails. Clearly, to understand the physical processes that drive changes in export production, seasonal and regional differences have to be considered as MLD does not consistently change in one direction throughout the year in the entire Southern Ocean. Biological production, however, is highly seasonal and physical changes in the growing season determine its response to climate change.

There is a strong need to understand the physical reasons for the models' different mixed layer depth (MLD) responses to climate change for all seasons in order to be able to make robust predictions about future export production and CO_2 uptake. This includes a thorough evaluation and possibly improvement of present-day MLD representation in the ocean models. It would also be highly desirable to have a common MLD definition in the next phases of CMIP and MAREMIP.

Acknowledgments
This research was supported through the Helmholtz Postdoc Programme and through the EU FP7 project CARBOCHANGE (grant agreement 264879). S. Doney and I. Lima were supported by the U.S. National Science Foundation through the Palmer LTER Project (NSF PLR-1440435). We acknowledge the World Climate Research Programme's Working Group on Coupled Modeling, which is responsible for CMIP. For CMIP the U.S. Department of Energy's Program for Climate Model Diagnosis and Intercomparison provides coordinating support and led development of software infrastructure in partnership with the Global Organization for Earth System Science Portals. We thank two reviewers for their constructive comments on the manuscript. All model outputs are available from either the CMIP5 (http://pcmdi9.llnl.gov/esgf-web-fe/) or MAREMIP (access to ftp server can be provided upon request, Taka Hirata: tahi@ees.hokudai.ac.jp) archives. In addition, the data used to produce the figures are available at http://dx.doi.org/10.1594/PANGAEA.849079.

References

Aumont, O., and L. Bopp (2006), Globalizing results from ocean in situ iron fertilization studies, *Global Biogeochem. Cycles*, *20*, GB2017, doi:10.1029/2005GB002591.

Bakker, D., H. D. Baar, and U. Bathmann (1997), Changes of carbon dioxide in surface waters during spring in the Southern Ocean, *Deep Sea Res. Part II*, *44*(1-2), 91–127, doi:10.1016/S0967-0645(96)00075-6.

Böning, C. W., A. Dispert, M. Visbeck, S. R. Rintoul, and F. U. Schwarzkopf (2008), The response of the Antarctic Circumpolar Current to recent climate change, *Nat. Geosci.*, *1*, 864–869, doi:10.1038/ngeo362.

Bopp, L., et al. (2013), Multiple stressors of ocean ecosystems in the 21st century: Projections with CMIP5 models, *Biogeosciences*, *10*(10), 6225–6245, doi:10.5194/bg-10-6225-2013.

Buitenhuis, E. T., T. Hashioka, and C. L. Quéré (2013), Combined constraints on global ocean primary production using observations and models, *Global Biogeochem. Cycles*, *27*(3), 847–858, doi:10.1002/gbc.20074.

Carranza, M. M., and S. T. Gille (2015), Southern Ocean wind-driven entrainment enhances satellite chlorophyll-*a* through the summer, *J. Geophys. Res. Oceans*, *120*, 304–323, doi:10.1002/2014JC010203.

Collins, W. J., et al. (2011), Development and evaluation of an Earth system model—HadGEM2, *Geosci. Model Dev.*, *4*(4), 1051–1075, doi:10.5194/gmd-4-1051-2011.

De Baar, H. J., J. T. De Jong, D. C. Bakker, B. M. Löscher, C. Veth, U. Bathmann, and V. Smetacek (1995), Importance of iron for plankton blooms and carbon dioxide drawdown in the Southern Ocean, *Nature*, *373*, 412–415, doi:10.1038/373412a0.

de Boyer Montégut, C., G. Madec, A. S. Fischer, A. Lazar, and D. Iudicone (2004), Mixed layer depth over the global ocean: An examination of profile data and a profile-based climatology, *J. Geophys. Res.*, *109*, C12003, doi:10.1029/2004JC002378.

de Lavergne, C., J. B. Palter, E. D. Galbraith, R. Bernardello, and I. Marinov (2014), Cessation of deep convection in the open Southern Ocean under anthropogenic climate change, *Nat. Clim. Change*, *4*(4), 278–282, doi:10.1038/NCLIMATE2132.

Downes, S. M., and A. M. Hogg (2013), Southern Ocean circulation and eddy compensation in CMIP5 models, *J. Clim.*, *26*, 7198–7220, doi:10.1175/JCLI-D-12-00504.1.

Dugdale, R., and J. Goering (1967), Uptake of new and regenerated forms of nitrogen in primary productivity1, *Limnol. Oceanogr.*, *12*(2), 196–206.

Dunne, J. P., et al. (2013), GFDL's ESM2 global coupled climate-carbon Earth system models. Part II: Carbon system formulation and baseline simulation characteristics, *J. Clim.*, *26*(7), 2247–2267, doi:10.1175/JCLI-D-12-00150.1.

Durack, P. J., and S. E. Wijffels (2010), Fifty-year trends in global ocean salinities and their relationship to broad-scale warming, *J. Clim.*, *23*(16), 4342–4362, doi:10.1175/2010JCLI3377.1.

Geider, R. J., H. L. MacIntyre, and T. M. Kana (1998), A dynamic regulatory model of phytoplankton acclimation to light, nutrients, and temperature, *Limnol. Oceanogr.*, *43*, 679–694, doi:10.4319/lo.1998.43.4.0679.

Gruber, N., et al. (2009), Oceanic sources, sinks, and transport of atmospheric CO_2, *Global Biogeochem. Cycles*, *23*, GB1005, doi:10.1029/2008GB003349.

Hashioka, T., M. Vogt, Y. Yamanaka, C. Le Quéré, E. T. Buitenhuis, M. N. Aita, S. Alvain, L. Bopp, T. Hirata, I. Lima, S. Sailley, and S. C. Doney (2013), Phytoplankton competition during the spring bloom in four plankton functional type models, *Biogeosciences*, *10*(11), 6833–6850, doi:10.5194/bg-10-6833-2013.

Hauck, J., and C. Völker (2015), Rising atmospheric CO_2 leads to large impact of biology on Southern Ocean CO_2 uptake via changes of the Revelle factor, *Geophys. Res. Lett.*, *42*, 1459–1464, doi:10.1002/2015GL063070.

Hauck, J., C. Völker, T. Wang, M. Hoppema, M. Losch, and D. A. Wolf-Gladrow (2013), Seasonally different carbon flux changes in the Southern Ocean in response to the southern annular mode, *Global Biogeochem. Cycles*, *27*(4), 1236–1245, doi:10.1002/2013GB004600.

Haumann, F. A., D. Notz, and H. Schmidt (2014), Anthropogenic influence on recent circulation-driven Antarctic sea ice changes, *Geophys. Res. Lett.*, *41*, 8429–8437, doi:10.1002/2014GL061659.

Hoppema, M. (2004), Weddell Sea turned from source to sink for atmospheric CO_2 between pre-industrial time and present, *Global Planet. Change*, *40*, 219–231, doi:10.1016/j.gloplacha.2003.08.001.

Ito, T., A. Bracco, C. Deutsch, H. Frenzel, M. Long, and Y. Takano (2015), Sustained growth of the Southern Ocean carbon storage in a warming climate, *Geophys. Res. Lett.*, *42*, 4516–4522, doi:10.1002/2015GL064320.

Kara, A. B., P. A. Rochford, and H. E. Hurlburt (2000), An optimal definition for ocean mixed layer depth, *J. Geophys. Res.*, *105*(C7), 16,803–16,821, doi:10.1029/2000JC900072.

Khatiwala, S., F. Primeau, and T. Hall (2009), Reconstruction of the history of anthropogenic CO_2 concentrations in the ocean, *Nature*, *462*, 346–349, doi:10.1038/nature08526.

Khatiwala, S., T. Tanhua, S. Mikaloff Fletcher, M. Gerber, S. C. Doney, H. D. Graven, N. Gruber, G. A. McKinley, A. Murata, A. F. Ríos, and C. L. Sabine (2013), Global ocean storage of anthropogenic carbon, *Biogeosciences*, *10*(4), 2169–2191, doi:10.5194/bg-10-2169-2013.

Large, W. G., G. Danabasoglu, S. C. Doney, and J. C. McWilliams (1997), Sensitivity to surface forcing and boundary layer mixing in a global ocean model: Annual-mean climatology, *J. Phys. Oceanogr.*, *27*(11), 2418–2447.

Laufkötter, C., et al. (2015), Drivers and uncertainties of future global marine primary production in marine ecosystem models, *Biogeosci. Discuss.*, *12*(4), 3731–3824, doi:10.5194/bgd-12-3731-2015.

Law, R. M., R. J. Matear, and R. J. Francey (2008), Comment on: "Saturation of the Southern Ocean CO_2 sink due to recent climate change", *Science*, *319*, 570a, doi:10.1126/science.1149077.

Le Quéré, C., et al. (2007), Saturation of the Southern Ocean CO_2 sink due to recent climate change, *Science*, *316*, 1735–1738, doi:10.1126/science.1136188.

Le Quéré, C., et al. (2008), Response to Comments on "Saturation of the Southern Ocean CO_2 sink due to recent climate change", *Science*, *319*, 570c, doi:10.1126/science.1147315.

Lenton, A., and R. J. Matear (2007), Role of the Southern Annular Mode (SAM) in Southern Ocean CO_2 uptake, *Global Biogeochem. Cycles*, *21*, GB2016, doi:10.1029/2006GB002714.

Lenton, A., et al. (2013), Sea-air CO_2 fluxes in the Southern Ocean for the period 1990–2009, *Biogeosciences*, *10*, 4037–4054, doi:10.5194/bg-10-4037-2013.

Lovenduski, N. S., N. Gruber, S. C. Doney, and I. D. Lima (2007), Enhanced CO_2 outgassing in the Southern Ocean from a positive phase of the Southern Annular Mode, *Global Biogeochem. Cycles*, *21*, GB2026, doi:10.1029/2006GB002900.

Marinov, I., A. Gnanadesikan, J. Toggweiler, and J. Sarmiento (2006), The Southern Ocean biogeochemical divide, *Nature*, *441*(7096), 964–967, doi:10.1038/nature04883.

Marinov, I., S. C. Doney, I. D. Lima, K. Lindsay, J. K. Moore, and N. Mahowald (2013), North-South asymmetry in the modeled phytoplankton community response to climate change over the 21st century, *Global Biogeochem. Cycles*, *27*(4), 1274–1290, doi:10.1002/2013GB004599.

Marshall, G. J. (2003), Trends in the Southern Annular Mode from observations and reanalyses, *J. Clim.*, *16*, 4134–4143.

Marshall, J., and K. Speer (2012), Closure of the meridional overturning circulation through Southern Ocean upwelling, *Nat. Geosci.*, *5*, 171–180, doi:10.1038/ngeo1391.

Meijers, A. (2014), The Southern Ocean in the Coupled Model Intercomparison Project phase 5, *Philos. Trans. R. Soc. A*, *372*(2019), 20130,296, doi:10.1098/rsta.2013.0296.

Meinshausen, M., et al. (2011), The RCP greenhouse gas concentrations and their extensions from 1765 to 2300, *Clim. Change*, *109*(1-2), 213–241, doi:10.1007/s10584-011-0156-z.

Meredith, M. P., A. C. Naveira Garabato, A. M. Hogg, and R. Farnetti (2012), Sensitivity of the overturning circulation in the Southern Ocean to decadal changes in wind forcing, *J. Clim.*, *25*, 99–110, doi:10.1175/2011JCLI4204.1.

Michaelis, L., and M. L. Menten (1913), Die Kinetik der Invertinwirkung, *Biochem. Z*, *49*, 333–369.

Mikaloff Fletcher, S. E., et al. (2006), Inverse estimates of anthropogenic CO_2 uptake, transport, and storage by the ocean, *Global Biogeochemical Cycles*, *20*, GB2002, doi:10.1029/2005GB002530.

Mikaloff Fletcher, S. E., et al. (2007), Inverse estimates of the oceanic sources and sinks of natural CO_2 and the implied oceanic carbon transport, *Global Biogeochem. Cycles*, *21*, GB1010, doi:10.1029/2006GB002751.

Misumi, K., K. Lindsay, J. K. Moore, S. C. Doney, F. O. Bryan, D. Tsumune, and Y. Yoshida (2014), The iron budget in ocean surface waters in the 20th and 21st centuries: Projections by the community Earth system model version 1, *Biogeosciences*, *11*(1), 33–55, doi:10.5194/bg-11-33-2014.

Moore, J. K., K. Lindsay, S. C. Doney, M. C. Long, and K. Misumi (2013), Marine ecosystem dynamics and biogeochemical cycling in the community Earth system model [CESM1 (BGC)]: Comparison of the 1990s with the 2090s under the RCP4. 5 and RCP8. 5 Scenarios, *J. Clim.*, *26*(23), 9291–9312, doi:10.1175/JCLI-D-12-00566.1.

Orr, J., R. Najjar, C. L. Sabine, and F. Joos (1999), Abiotic-HOWTO, *Tech. Rep.*

Orsi, A., G. Johnson, and J. Bullister (1999), Circulation, mixing, and production of Antarctic Bottom Water, *Prog. Oceanogr.*, *43*(1), 55–109, doi:10.1016/S0079-6611(99)00004-X.

Purkey, S. G., and G. C. Johnson (2013), Antarctic bottom water warming and freshening: Contributions to sea level rise, ocean freshwater budgets, and global heat gain, *J. Clim.*, *26*(16), 6105–6122, doi:10.1175/JCLI-D-12-00834.1.

Rignot, E., J. L. Bamber, M. R. Van Den Broeke, C. Davis, Y. Li, W. J. Van De Berg, and E. Van Meijgaard (2008), Recent Antarctic ice mass loss from radar interferometry and regional climate modelling, *Nat. Geosci.*, *1*(2), 106–110, doi:10.1038/ngeo102.

Roy, T., L. Bopp, M. Gehlen, B. Schneider, P. Cadule, T. L. Frölicher, J. Segschneider, J. Tjiputra, C. Heinze, and F. Joos (2011), Regional impacts of climate change and atmospheric CO_2 on future ocean carbon uptake: A multimodel linear feedback analysis, *J. Clim.*, *24*(9), 2300–2318, doi:10.1175/2010JCLI3787.1.

Russell, J. L., K. W. Dixon, A. Gnanadesikan, R. J. Stouffer, and J. Toggweiler (2006), The Southern Hemisphere westerlies in a warming world: Propping open the door to the deep ocean, *J. Clim.*, *19*(24), 6382–6390, doi:10.1175/JCLI3984.1.

Sabine, C. L., et al. (2004), The oceanic sink for anthropogenic CO_2, *Science*, *305*(5682), 367–371, doi:10.1126/science.1097403.

Sailley, S., M. Vogt, S. Doney, M. Aita, L. Bopp, E. Buitenhuis, T. Hashioka, I. Lima, C. L. Quéré, and Y. Yamanaka (2013), Comparing food web structures and dynamics across a suite of global marine ecosystem models, *Ecol. Modell.*, *261-262*, 43–57, doi:10.1016/j.ecolmodel.2013.04.006.

Sallée, J. B., K. G. Speer, and S. R. Rintoul (2010), Zonally asymmetric response of the Southern Ocean mixed-layer depth to the Southern Annular Mode, *Nat. Geosci.*, *3*, 273–279, doi:10.1038/NGEO812.

Sallée, J.-B., E. Shuckburgh, N. Bruneau, A. Meijers, T. Bracegirdle, and Z. Wang (2013), Assessment of Southern Ocean mixed-layer depths in CMIP5 models: Historical bias and forcing response, *J. Geophys. Res. Oceans*, *118*(4), 1845–1862, doi:10.1002/jgrc.20157.

Sarmiento, J., N. Gruber, M. Brzezinski, and J. Dunne (2004), High-latitude controls of thermocline nutrients and low latitude biological productivity, *Nature*, *427*(6969), 56–60, doi:10.1038/nature02127.

Sarmiento, J. L., J. C. Orr, and U. Siegenthaler (1992), A perturbation simulation of CO_2 uptake in an ocean general circulation model, *J. Geophys. Res.*, *97*(C3), 3621–3645, doi:10.1029/91JC02849.

Séférian, R., L. Bopp, M. Gehlen, J. C. Orr, C. Ethé, P. Cadule, O. Aumont, D. S. y Mélia, A. Voldoire, and G. Madec (2013), Skill assessment of three Earth system models with common marine biogeochemistry, *Clim. Dyn.*, *40*(9-10), 2549–2573, doi:10.1007/s00382-012-1362-8.

Shigemitsu, M., T. Okunishi, J. Nishioka, H. Sumata, T. Hashioka, M. N. Aita, S. L. Smith, N. Yoshie, N. Okada, and Y. Yamanaka (2012), Development of a one-dimensional ecosystem model including the iron cycle applied to the Oyashio region, western subarctic Pacific, *J. Geophys. Res.*, *117*, C06021, doi:10.1029/2011JC007689.

Sloyan, B. M., and S. R. Rintoul (2001), Circulation, renewal, and modification of Antarctic mode and intermediate water, *J. Phys. Oceanogr.*, *31*, 1005–1030.

Smetacek, V., et al. (2012), Deep carbon export from a Southern Ocean iron-fertilized diatom bloom, *Nature*, *487*(7407), 313–319, doi:10.1038/nature11229.

Smith, S. L., Y. Yamanaka, M. Pahlow, and A. Oschlies (2009), Optimal uptake kinetics: Physiological acclimation explains the pattern of nitrate uptake by phytoplankton in the ocean, *Mar. Ecol. Prog. Ser.*, *384*, 1–12, doi:10.3354/meps08022.

Swart, N. C., and J. C. Fyfe (2012), Observed and simulated changes in the Southern Hemisphere surface westerly wind-stress, *Geophys. Res. Lett.*, *39*, L16711, doi:10.1029/2012GL052810.

Takahashi, T., et al. (2002), Global sea-air CO_2 flux based on climatological surface ocean pCO_2, and seasonal biological and temperature effects, *Deep Sea Res. Part II*, *49*(9-10), 1601–1622, doi:10.1016/S0967-0645(02)00003-6.

Taylor, K. E., R. J. Stouffer, and G. A. Meehl (2012), An overview of CMIP5 and the experiment design, *Bull. Am. Meteorol. Soc.*, *93*, 485–498, doi:10.1175/BAMS-D-11-00094.1.

Thompson, D. W. J., S. Solomon, P. J. Kushner, M. H. England, K. M. Grise, and D. J. Karoly (2011), Signatures of the Antarctic ozone hole in Southern Hemisphere surface climate change, *Nat. Geosci.*, *4*, 741–749, doi:10.1038/ngeo1296.

van Heuven, S. M., M. Hoppema, E. M. Jones, and H. J. d. Baar (2014), Rapid invasion of anthropogenic CO_2 into the deep circulation of the Weddell Gyre, *Philos. Trans. R. Soc. A*, *372*(2019), 20130,056, doi:10.1098/rsta.2013.0056.

Venables, H., and C. M. Moore (2010), Phytoplankton and light limitation in the Southern Ocean: Learning from high-nutrient, high-chlorophyll areas, *J. Geophys. Res.*, *115*, C02015, doi:10.1029/2009JC005361.

Verdy, A., S. Dutkiewicz, M. J. Follows, J. Marshall, and A. Czaja (2007), Carbon dioxide and oxygen fluxes in the Southern Ocean: Mechanisms of interannual variability, *Global Biogeochem. Cycles*, *21*, GB2020, doi:10.1029/2006GB002916.

Vogt, M., et al. (2013), The distribution, dominance patterns and ecological niches of plankton functional types in Dynamic Green Ocean Models and satellite estimates, *Biogeosci. Discuss.*, *10*(11), 17,193–17,247, doi:10.5194/bgd-10-17193-2013.

Wanninkhof, R. (1992), Relationship between wind speed and gas exchange over the ocean, *J. Geophys. Res.*, *97*, 7373–7382, doi:10.1029/92JC00188.

Zheng, F., J. Li, R. T. Clark, and H. C. Nnamchi (2013), Simulation and projection of the Southern Hemisphere annular mode in CMIP5 models, *J. Clim.*, *26*(24), 9860–9879, doi:10.1175/JCLI-D-13-00204.1.

Zickfeld, K., J. C. Fyfe, M. Eby, and A. J. Weaver (2008), Comment on "Saturation of the Southern Ocean CO_2 sink due to recent climate change", *Science*, *319*, 570b, doi:10.1126/science.1146886.